# Accelerated computer-aided screening of optical materials: Investigating the potential of $\Delta$ -SCF Methods to predict emission maxima of large dye molecules

Vikrant Tripathy, Amar Flood, Krishnan Raghavachari\*

Department of Chemistry, Indiana University, Bloomington, Indiana 47405, United States

#### **Abstract**

Accurate simulation of electronic excited states of large chromophores is often difficult due to the computationally expensive nature of existing methods. Common approximations such as fragmentation methods that are routinely applied to ground-state calculations of large molecules are not easily applicable to excited states due to the delocalized nature of electronic excitations in most practical chromophores. Thus, special techniques specific for excited states are needed. Δ-SCF methods are one such approximation that treats excited states in a manner analogous to ground state calculations, accelerating the simulation of excited states. In this work, we employed the popular initial maximum overlap method (IMOM) to avoid variational collapse of the electronic excited state orbitals to the ground state. We demonstrate that it is possible to obtain emission energies from the first singlet (S<sub>1</sub>) excited state of many thousands of dye molecules without any external intervention. Spin correction was found to be necessary to obtain accurate excitation and emission energies. Using thousands of dye-like chromophores and various solvents (12,318 combinations) we show that spin-corrected initial maximum overlap method (SC-IMOM) accurately predicts emission maxima with a mean absolute error (MAE) of only 0.27 eV. We further improved the predictive accuracy using linear fit-based corrections from individual dye classes to achieve an impressive performance of 0.17 eV. Additionally, we demonstrate that IMOM spin density can be used to identify the dye class of chromophores, enabling improved prediction accuracy for complex dye molecules such as dyads (chromophores containing moieties from two different dye classes). Finally, the convergence behavior of IMOM excited state SCF calculations is analyzed briefly to identify the chemical space where IMOM is more likely to fail.

Corresponding Author: Krishnan Raghavachari, e-mail: kraghava@indiana.edu

### 1. Introduction

Modern optical materials can be developed and tuned to achieve specialized goals. <sup>1-3</sup> Small-molecule ionic isolation lattices (SMILES)<sup>1</sup> represent one such recent example that solves the longstanding <sup>4,5</sup> issue of self-quenching of fluorescence in high-density solid-state materials. The SMILES materials have the unique ability to turn on the fluorescence of dyes in solid-state materials, thereby broadening the scope of potential applications. <sup>6,7</sup> Initial observations <sup>1</sup> on SMILES materials have suggested certain rules must be followed by the dye molecules for optimal performance. This rule-based approach has opened the door for theoretical investigations that prescreen dye molecules to accelerate the design, synthesis, and discovery of novel optical materials with desirable properties. <sup>8,9</sup> The rules that need to be screened include properties such as redox potentials, excitation and emission energies, singlet-triplet gap, etc., and they depend on the specific application being considered. Among these properties, evaluation of the emission energy is considered one key bottleneck since it is a property of the excited state and requires optimization of the excited state geometry.

The study of excited states poses a significant challenge in computational chemistry. Electronic excited states are purely quantum mechanical in nature, and typically start from a solution of the ground state solution. This situation makes these calculations more expensive and, in many cases, significantly more challenging to perform for large molecules. Highly accurate methods like EOMCC<sup>10</sup> and CASSCF<sup>11</sup> can only be applied to smaller molecules due to their steep computational scaling with system size. There have been some notable attempts applying such methods to large molecules but, routine application is not practical.<sup>12,13</sup> The most widely used method, time-dependent density functional theory (TDDFT),<sup>14</sup> provides a reasonable compromise between cost and accuracy for standard use with medium-sized molecules. Using this method, vertical excitation energies (at the ground state geometry) can be routinely obtained for molecules of the size of 100 atoms. However, the calculation of more complex properties of excited states, such as, emission spectra (requiring excited state optimization) are still expensive, limiting the range of application while increasing the cost of screening dye molecules.

Δ-SCF methods have long been used to obtain excitation energies, well before the advent of linear response methods like TDDFT.<sup>15,16</sup> These methods obtain the excitation energy as the difference between the energy of two separate calculations, one each for the ground and excited

states. The application of such methods is straightforward for transitions to the lowest electronic excited states involving a different symmetry from the ground state. However, this approach often fails if the excited state is not the lowest energy of a given symmetry, resulting in variational collapse. A few different formulations such as, relaxing virtual orbitals,  $^{17-19}$  relaxing both virtual and occupied orbitals among themselves,  $^{20}$  level shifting of virtual orbitals $^{21}$  and saddle points of electronic energy have been proposed to circumvent this issue. The maximum overlap method (MOM) by Gill *et al.* overcomes this issue by populating states based on the overlap of new orbitals with old ones. This process leads to a non-Aufbau electronic configuration for the excited state, avoiding variational collapse in many cases. A more robust method called initial maximum overlap method (IMOM) was proposed later, which improved its convergence significantly. These new generations of  $\Delta$ -SCF methods have mostly been developed for application to problems where TDDFT fails, such as doubly excited states,  $^{24-26}$  Rydberg excited states,  $^{24,27}$  core excitation,  $^{28,29}$  and conical intersections. However, the computational efficiency of such methods over TDDFT has not been the focus of attention in most studies.

Kowalczyk *et al.* assessed the performance of Δ-SCF methods for electronic excitations in a small set of 16 of different dye molecules and demonstrated performance similar to TDDFT.<sup>31</sup> In the current work, we show the successful application of IMOM to a large number of dye molecules (over 4500) belonging to a variety of popular dye classes with a focus on emission maxima (more computationally expensive than excitation energy). Two different datasets were employed for our analysis. Our initial tests were focused on a relatively smaller subset of data obtained from PhotoChemCAD 3,<sup>32</sup> containing 339 different dye molecules belonging to 20 different families. Out of these dye molecules, only 214 had available emission data from 19 different dye classes. Seven of these molecules had convergence issues while doing excited state optimizations with IMOM and two of them were too large to perform TDDFT optimizations. Thus, our first dataset consisted of 205 molecules (**Figure 1**). The different dye types are annotated in different colors. We will follow this color scheme later while analyzing the performance of IMOM. These molecules contain common chromophores such as cyanines, xanthenes, porphyrins, etc., and they

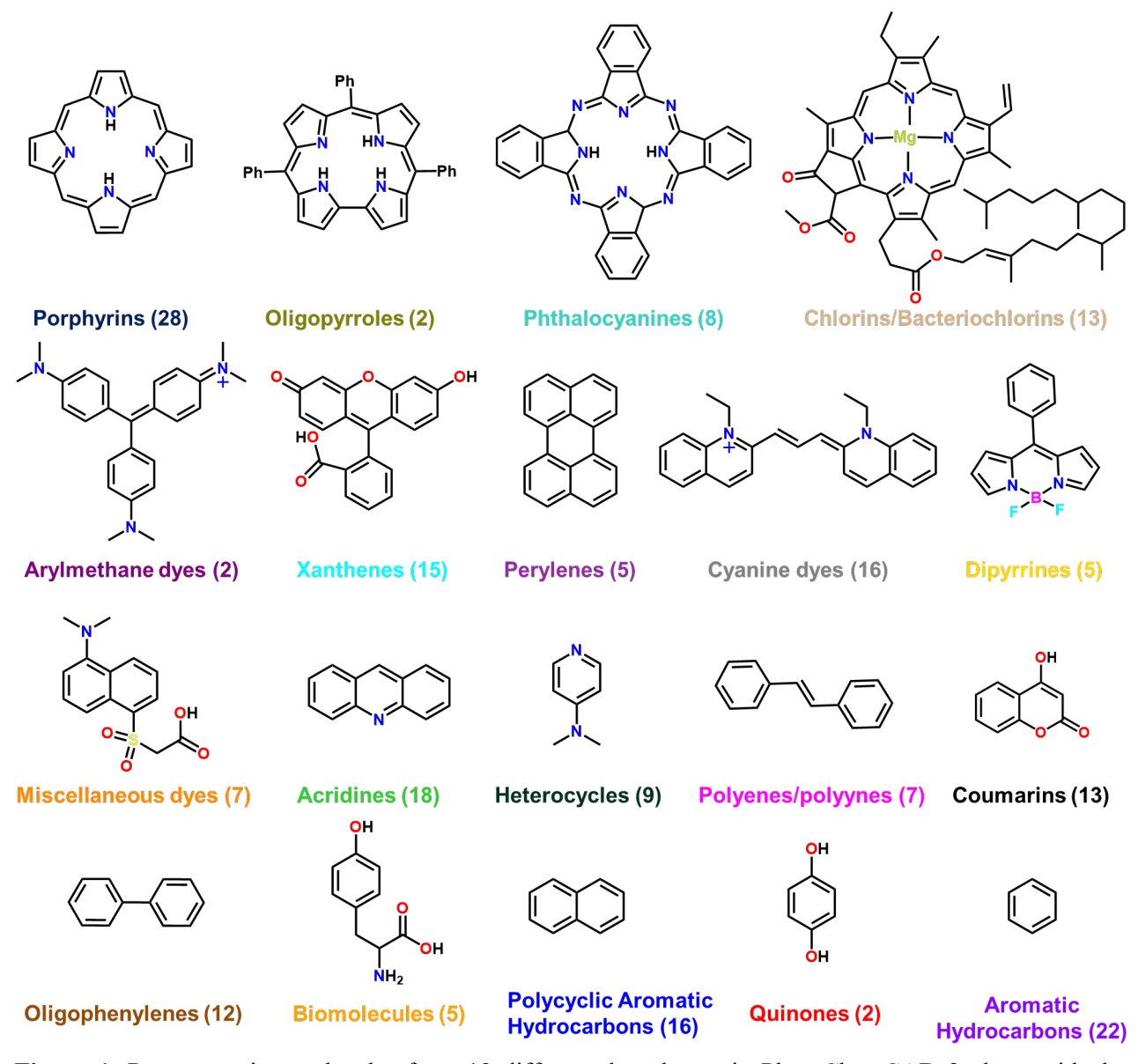


**Figure 1**: Representative molecules from 19 different dye classes in PhotoChemCAD 3 along with the number of molecules from each class in our dataset (in brackets). In total, 205 molecules are considered in our dataset. This dataset is called PCAD-dataset in this article.

range in size from small to large containing up to 181 atoms, forming a good quality test set, called the PCAD-dataset, for showing the scope of the application.

Even though the PCAD-dataset contains common chromophores, it is small compared to the chemical space of potential dyes. Several larger datasets<sup>33-36</sup> are now available due to the explosion of machine learning for the virtual high-throughput screening of dye molecules.<sup>37-39</sup> However, a majority of these datasets consist of small organic molecules with unknown optical properties.

Typically, these models generally use excitation energies from TDDFT, xTB-sTDA,<sup>40</sup> or CC2<sup>41</sup> calculations as reference values. More recently, Joung *et al.* compiled a large database of optical properties of organic molecules containing a total of 20,236 data points comprised of 7,016 unique chromophores in 365 solvents or in the solid state.<sup>42</sup> Our second large dataset is a subset of this collection chosen using a filtering procedure (**Figure 2**). Since we will be performing excited state optimizations, we placed a few restrictions on the size of molecules, availability of solvent parameters, closed shell molecules, availability of non-conflicting experimental emission data, etc. The final subset of 12,318 datapoints comprising 4,487 unique chromophores and 69 solvents is called the Large-dataset.

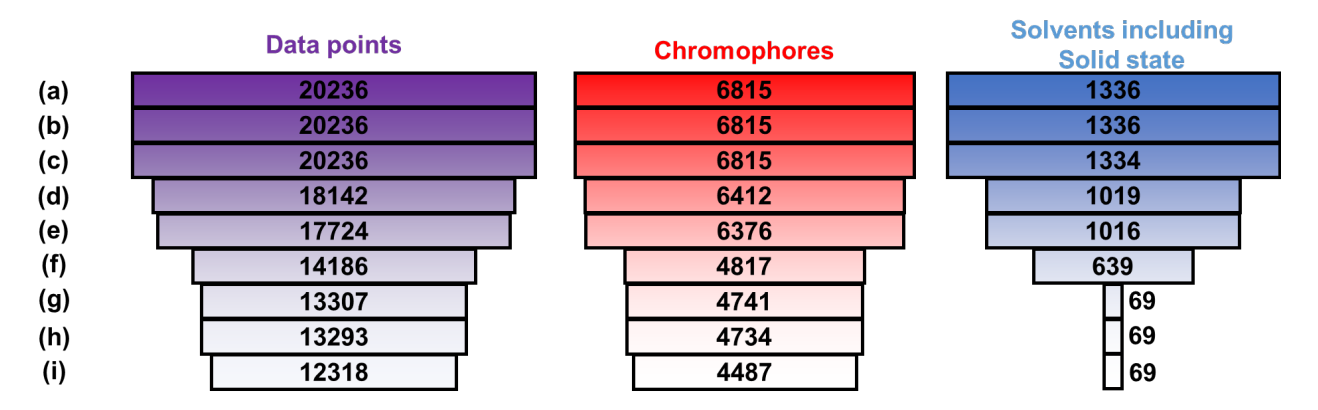


**Figure 2:** Procedure for dataset curation. (a) Original dataset from Ref 42 (SMILES<sup>43</sup> strings of chromophores and solvents), (b) removing counter-ions and solvent from chromophore SMILES strings, (c) replacing deuterated solvents with their protonated analogues such as water ( $H_2O$ ) in place of its deuterated analog ( $D_2O$ ), (d) discarding data points with no emission data, (e) removing data points with conflicting data, i.e., if multiple data points are present corresponding to the same chromophore-solvent combination but, they have different reported emission maxima, (f) capping chromophores size to 80 atoms, (g) remove datapoints with parameters not available in Gaussian, (h) removing radicals and  $C_{70}$ , and (i) discarding datapoints with convergence issues while performing IMOM calculations (*vide infra*).

Using the PCAD-dataset (205 dyes), we show that the excited states obtained using a spin-corrected version of IMOM (SC-IMOM) match those from TDDFT. Further, we show that the true strength of  $\Delta$ -SCF methods is in the calculation of excited state gradients required to obtain emission energies. Leveraging this aspect of  $\Delta$ -SCF methods and the unique property of IMOM for furnishing excited state wavefunctions, we obtain emission maxima of these large dye molecules and compare them to their corresponding experimental values. Using the Large-dataset (4,487 dyes and 12,318 dye-solvent combinations), we show that our assertions are generally

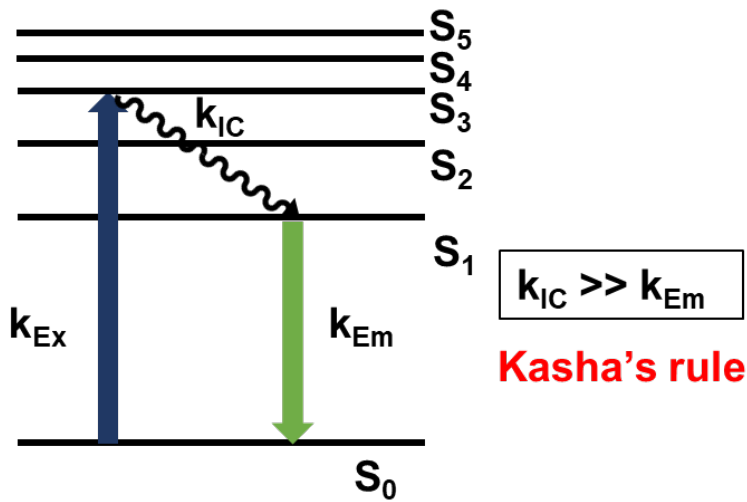


**Figure 3**: Simplified Jablonski diagram denoting the excitation and emission phenomena.

applicable to a broad range of dye molecules. All counterions of the dye molecules were removed while performing calculations.

#### 2. Methods

All calculations were performed using a modified version of Gaussian<sup>44</sup> at B3LYP-D3BJ/Def2SVP level of theory. 45, 46 While the basis set is modest, the performance of a larger basis set (Def2TZVP) was found to be essentially identical (vide infra). Additionally, the use of a smaller basis set permits the screening of many thousands of candidates at a consistent level of theory, and the results (vide infra) are surprisingly good. The spin corrections were performed using an external Perl script interface. Our own implementation enabled us to have better control over our analysis and will facilitate further developments in the future. First, the ground state structures were optimized and confirmed to be minima using a frequency analysis, followed by excited state optimizations for emission. Excitation energies were obtained at the ground state (S<sub>0</sub>) geometry. Emission energies were obtained at the first excited state (S<sub>1</sub>) geometry since the rate of internal conversion (k<sub>IC</sub>) is generally much faster than rate of emission (k<sub>Em</sub>) as per Kasha's rule, 47 as illustrated by a representative Jablonski diagram in Figure 3. The initial ground state structures for the Large-dataset were obtained automatically by first performing a conformational search (python script provided along with the supplementary information), followed by single point DFT (B3LYP-D3BJ/Def2SVP) calculations to obtain the lowest energy conformer. The lowest energy conformer is optimized and confirmed to be a minimum using frequency analysis.

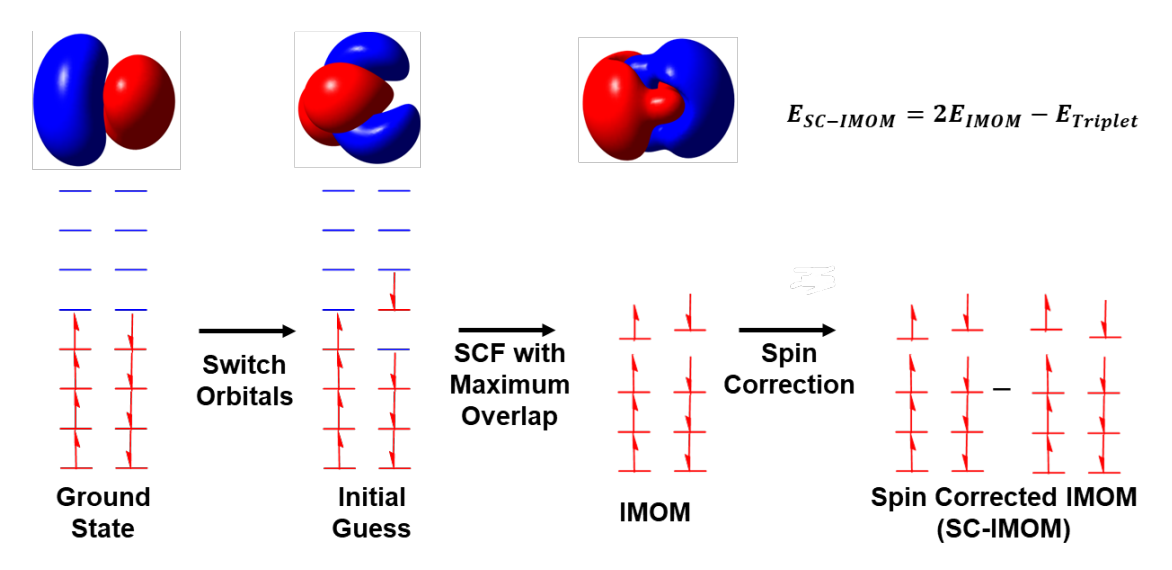
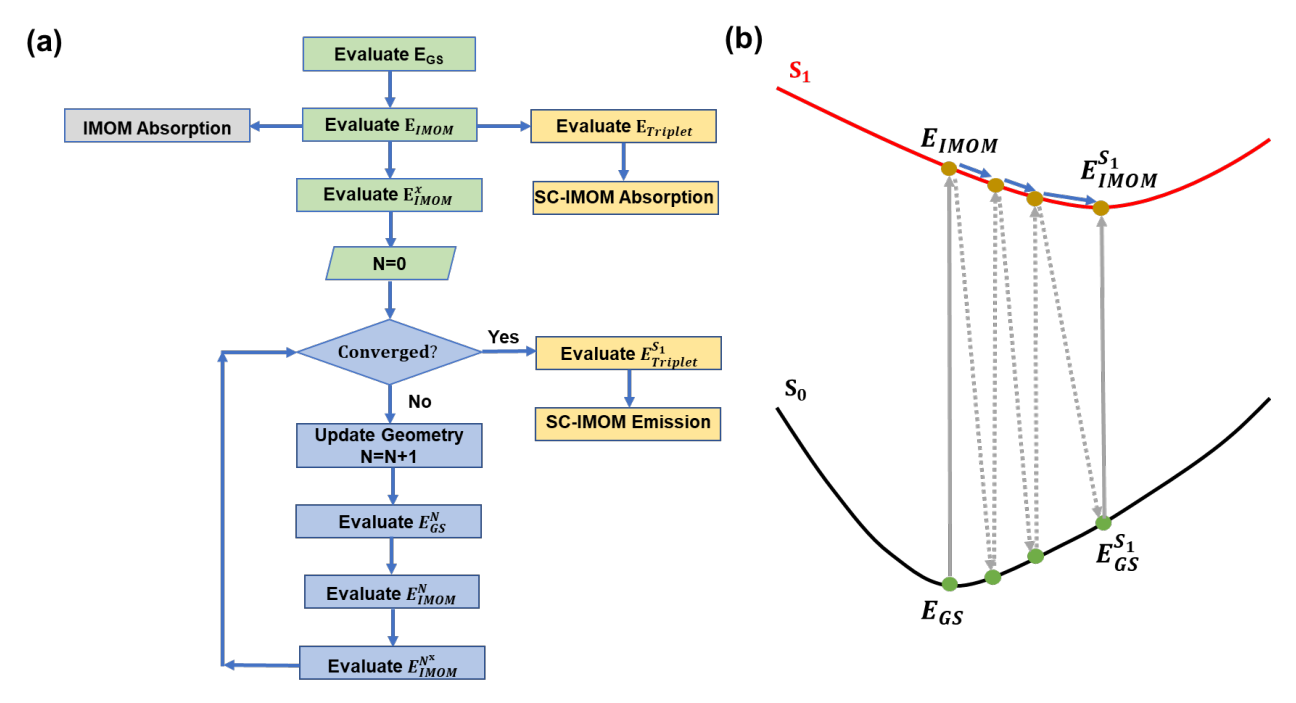


Figure 4: Workflow for performing IMOM and its spin corrected version SC-IMOM.

Excited state calculations were performed using both TDDFT and IMOM. Since all the molecules considered have closed shell electronic configuration, ground state structures were obtained by calculations using a "restricted" formalism. However, the excited state calculations use restricted and unrestricted formalisms for TDDFT and IMOM, respectively. Unrestricted wavefunctions were necessary for IMOM to enable switching of orbitals to obtain the initial guess as shown in **Figure 4**. IMOM avoids variational collapse to the ground state by obtaining the excited state as a non-Aufbau determinant using a maximum overlap condition. The excited state orbitals are obtained by maximizing the overlap of the occupied orbitals with the initial guess. The overlap of orbitals  $(O_i)$  is obtained as per **eq 1**. Electrons are filled in the orbitals in the order of most to least overlap. The excited state orbitals are non-orthogonal to those in the ground state. However, the excellent performance (*vide infra*) shows that this is not a critical factor.

$$O_i = \sum_{j \in occ} \left( \sum_{\mu,\nu} \left( C_{\nu j}^{guess} \right)^{\dagger} S_{\mu\nu} C_{\mu i}^{current} \right)^2 \tag{1}$$

The IMOM excited states correspond to broken spin symmetry solutions. The triplet contribution to the excitation energy can be approximately removed by using the spin correction of Ziegler *et al.*<sup>48</sup> (**eq 2**) and is applied to obtain the "spin-corrected" singlet energies. If needed, the composite energy from **eq 2** can be used to optimize the geometry of the spin-corrected singlet,



**Figure 5**: (a) The workflow followed in this work in obtaining the  $\Delta$ -SCF (IMOM and SC-IMOM) absorption and emission energies. (b) Schematics of approach where, the solid (blue) arrow represents the steps taken i.e., we are probing the excited state and the dotted arrows represent the actual sequence of calculations. At each step we are performing both the ground state SCF and SCF using maximum overlap condition for the excited state. The SCF gradient is performed only for the excited state as we are probing the excited state potential energy surface.

but the effects were found to be small (**Figure S1**). The spin corrected  $\Delta$ -SCF method will be called SC-IMOM throughout the rest of this article.

$$E_{SC-IMOM} = 2E_{IMOM} - E_{Triplet} \tag{2}$$

We apply our spin correction to both absorption and emission energies. The absorption energy is obtained at the ground state geometry. On the other hand, the emission energy is obtained at the excited state geometry. An appropriate workflow is designed and presented in **Figure 5a** and **Figure 5b** provides a pictorial illustration of our approach. For absorption, we perform both standard SCF and SCF using the maximum overlap condition to obtain  $E_{GS}$  and  $E_{IMOM}$  respectively. The IMOM and SC-IMOM absorption energies are obtained as per **eqs. 3** and **4** respectively.

$$IMOM \ Absorption = E_{IMOM} - E_{GS} \tag{3}$$

$$SC-IMOM\ Absorption = \left(2 \times E_{IMOM} - E_{Triplet}\right) - E_{GS}$$
 (4)

The IMOM excited state is optimized to obtain the excited state geometry for emission (**Figure 5b**). For optimization, steps were taken on the potential energy surface of the electronic excited state. In the initial implementation illustrated in **Figure 5b**, we performed ground state calculations at every step to obtain the guess for the excited state calculation using the maximum overlap condition. While the ground state calculation is clearly not needed for every step, we elected to do this in this initial study to avoid the collapse of the wavefunction to the ground state during the excited state optimization. Thus, every step in the excited state optimization consisted of three stages, viz. a standard SCF ground state calculation, an SCF for the excited state using maximum overlap condition, and excited state SCF gradient. Since all three are ground state-like calculations, this method is computationally efficient. Finally, we spin-corrected the emission energy as per **eq 5.** Here, the superscript S<sub>1</sub> denotes calculations carried out at the excited state geometry.

$$SC-IMOM\ Emission = \left(2 \times E_{IMOM}^{S_1} - E_{Triplet}^{S_1}\right) - E_{GS}^{S_1}$$
 (5)

There are two important conditions for the success of the IMOM and SC-IMOM models used in this work. (1) The converged excited state should be a broken symmetry singlet state with singlet and triplet states having close to equal contribution. This requirement was found to be satisfied for our test set using B3LYP as very few molecules had convergence issues (*vide infra*) with  $\langle S^2 \rangle$  values of the rest of the molecules lying between 0.9 and 1.1 all through the optimization process ( $\langle S^2 \rangle = 1$  indicates equal mixing of singlet and triplet). (2) Usage of appropriate initial guess, i.e., choice of orbitals to switch. Since we are aiming to predict experimental emission energies, we will be restricting ourselves to the first singlet excited state (S<sub>1</sub>). The choice of first singlet excited state relies on Kasha's rule. Thus, the only orbital switching we will perform involves the HOMO and LUMO orbitals, simplifying the process. This approach also helps to show that  $\Delta$ -SCF methods can be applied in a black-box manner by eliminating the need for human intervention specifically in the choice of orbitals to switch to obtain the initial guess. **Figure S2** demonstrates that other initial guesses, such as HOMO-1 to LUMO and HOMO to LUMO+1 produce higher excited states for all 205 molecules in the test set. Thus, the HOMO-LUMO switch will be considered default for IMOM and SC-IMOM throughout the rest of the article.

### 3. Results and Discussion

## 3.1 Assessment of the performance using the PCAD-dataset

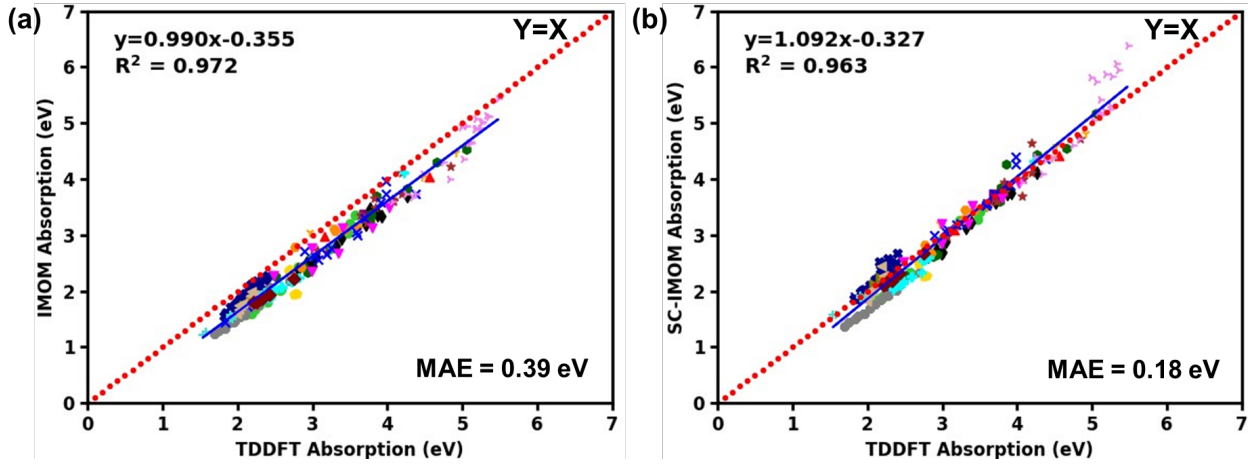


**Figure 6**: Comparison of absorption energies for (a) IMOM and (b) the spin corrected version (SC-IMOM) with respect to TDDFT. The PCAD-dataset is used in this analysis. The color coding is according to **Figure 1**. The red dotted line indicates the Y=X line.

We begin with analyzing the importance of spin correction to IMOM energies. Figure 6 compares the TDDFT excitation energies of the PCAD-dataset corresponding to S<sub>1</sub> excited state with IMOM (without spin correction) and SC-IMOM (with spin correction) in Figure 6a and Figure 6b, respectively. Each of the different dye types are color coded (see Figure 1). To test the accuracy of IMOM in obtaining excitation (absorption) energies, we used the well-established method, TDDFT, as the reference value. IMOM systematically underestimates the excitation energies for the whole dataset with a mean absolute error (MAE) of 0.39 eV. Despite the underestimation, the correlation was still high with R<sup>2</sup> value of 0.97 using linear regression. The best fit line was also found to be approximately parallel to the Y=X line with a slope of 0.99. This systematic underestimation could be attributed to the contamination of the IMOM excited singlet states from triplet excited states. This contamination is due to the wavefunction (Figure 4) not being an eigenstate of the S<sup>2</sup> operator. The excited state obtained by IMOM has biradical character (two unpaired spins with  $\langle S^2 \rangle \approx 1$ ), as illustrated in the wavefunction shown in **Figure 4**. However, the TDDFT excited state is a pure singlet. Since we are interested in singlet excited states, the triplet contribution needs to be filtered out. The coupling of the two spins (J) in a diradical (two unpaired spins) can be written as per eq 6.

$$J = \frac{1}{2} [E_{singlet} - E_{triplet}] \tag{6}$$

Spin contamination is a common occurrence in the study of low-spin metal complexes using the efficient single-reference DFT method. Thus, several workers<sup>49-51</sup> have investigated methods

to remove the spin contamination or estimate the coupling constant (J) of magnetic centers. Yamaguchi *et al.* provided one such approach that approximately projects out the spin contamination of a general broken symmetry (BS) state using the high spin state (HS) as per **eq** 7.50 This method needs only two different calculations, one at broken symmetry (not a spin eigenstate) and one with high-spin state (triplet for our purpose). The high spin state is employed due to the near absence of spin contamination in that state.

$$J = \frac{(E_{BS} - E_{HS})}{(\langle S^2 \rangle_{HS} - \langle S^2 \rangle_{BS})} \tag{7}$$

A drawback of this method is that the analytic gradient of this method can be somewhat expensive as it scales closer to post-SCF methods. Since our IMOM excited states show biradical characteristics of  $\langle S^2 \rangle \approx 1$ , a simplification of eq 7 can be achieved. Considering our high spin state is a triplet, broken-symmetry state is IMOM, and utilizing their approximate  $\langle S^2 \rangle$  values of 2 and 1, the simplified form of eq 7 is presented in eq 8.

$$J = E_{IMOM} - E_{Triplet} \tag{8}$$

This relationship yields the approximate singlet (SC-IMOM) energy as per eq 2. The spin correction is shown to improve performance (Figure 6b) with a lower MAE of 0.18 eV compared

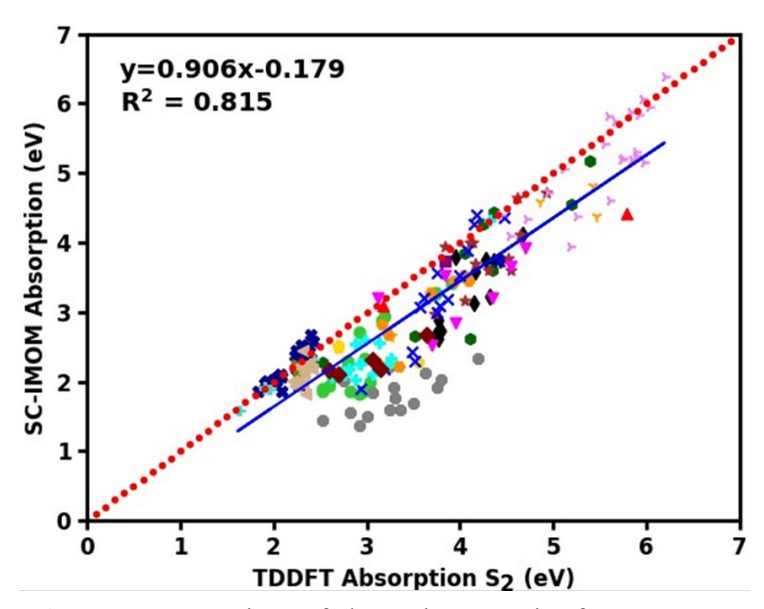


**Figure 7**: Comparison of absorption energies for SC-IMOM with respect to second singlet excited state (S<sub>2</sub>) of TDDFT. The PCAD-dataset is used for this. The color coding is according to **Figure 1**. The red dotted line indicates the Y=X line.

to the uncorrected IMOM. After correction, the correlation (R<sup>2</sup> value) remained high with a slope approximately parallel to Y=X line. The small decrease in correlation is due to the overestimation of absorption energies for aromatic hydrocarbons. This overestimation can be attributed to the excited states being too high in energy and the absorption spectrum lying in the UV region. Further, the high symmetry of these molecules results in excited states having non-negligible contributions from multiple one-electron excitations. This situation is not ideal for IMOM since it is a single determinant method and uses guess from switching an electron between two orbitals corresponding to a one-electron transition. Except for these small aromatic hydrocarbons, the SC-IMOM and TDDFT absorptions have similar excitation energies covering the entire visible region including the near UV.

To reinforce our assertions that the SC-IMOM energies obtained by HOMO-LUMO orbital switching correspond to the S<sub>1</sub> state, we compared them to the S<sub>2</sub> excited states obtained using TDDFT (**Figure 7**). The TDDFT S<sub>2</sub> state is generally found to be higher than SC-IMOM with a 0.54 eV MAE. The correlation was also significantly lower when compared to the S<sub>1</sub> state from TDDFT along with the linear regression line drifting away from the Y=X line. Thus, it can be said with reasonable certainty that the HOMO-LUMO orbital switching used in SC-IMOM reflects transitions to the S<sub>1</sub> excited state. However, this transition may not be the one with the highest oscillator strength. We tested this idea by comparing SC-IMOM absorption energies with the corresponding experimental values. The error is larger when the absorption energy is higher (**Figure S3**). This outcome is due to the absorption energy not corresponding to the lowest excited state (**Figures S4** and **S5**). Thus, prediction of absorption maxima using IMOM will require calculation of oscillator strengths and will be the topic of future investigation. Overall, the SC-IMOM energy corresponds to the S<sub>1</sub> excited state with two major implications. (1) This approach facilitates automation for large scale application (*vide infra*) and (2) emission energies can be obtained by optimizing the S<sub>1</sub> excited state as per Kasha's rule.<sup>47</sup>

The simple expression of the SC-IMOM energy in eq 2 allows for easy gradient formulation as a linear combination of IMOM and triplet gradients as carried out by Hanson-Heine *et al.*<sup>53, 54</sup> for a few coumarin dyes along with a test set of small molecules. They observed that the impact of spin correction was significantly greater for excitation energies than for geometry and vibrational frequencies. Our test calculations agreed with their observations (**Figure S1**). Thus,

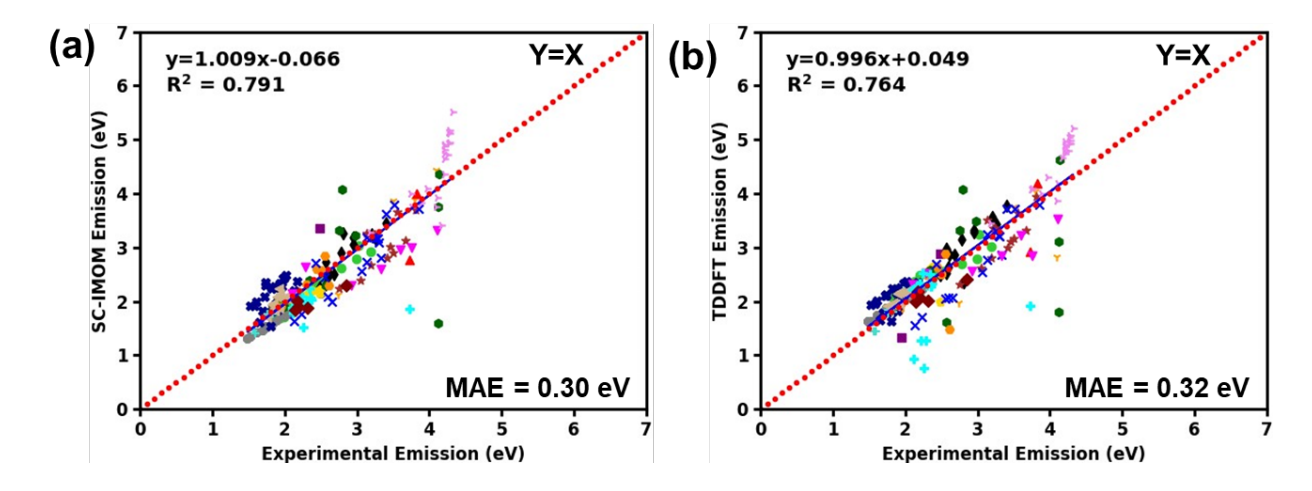


**Figure 8**: Comparison of emission energies for (a) SC-IMOM and (b) TDDFT with respect to experimental emission maxima. The PCAD-dataset is used for this. The color coding is according to **Figure 1**. The red dotted line indicates the Y=X line.

optimization of the S<sub>1</sub> excited state for emission was performed using IMOM instead of SC-IMOM. The use of IMOM was limited to obtaining the S<sub>1</sub> excited state geometry and SC-IMOM was used to get the emission energy. This approach has the added benefit of being cost effective. **Figure 8** presents the comparison between theoretically calculated emission compared to experimental emission maxima. Unlike absorption energies, here we compare the two theoretical methods, TDDFT and SC-IMOM, separately.

For the vast majority of cases, both methods perform equally well. Both TDDFT and SC-IMOM overestimate the emission energies of the high energy excited states of the aromatic hydrocarbons (light-pink data) with SC-IMOM estimation being higher. This outcome was expected from the results in **Figure 6b** where SC-IMOM absorption was higher than TDDFT. More importantly, SC-IMOM had significantly better performance in the lower excitation energy region consisting mainly of xanthenes, which are more valuable dyes for a variety of applications spanning from bioimaging <sup>55,56</sup> to optical materials. <sup>57</sup> Taken as a whole, SC-IMOM performed marginally better than TDDFT in predicting emission maxima. This finding is evident from a slightly lower MAE and higher correlation relative to the experimental value. The performance of SC-IMOM in obtaining emission maxima is found to be similar to the best-performing functional in the study of 101 excitation energy of 14 small organic molecules by Leang *et al.* (MAE ~0.3 eV). <sup>58</sup>

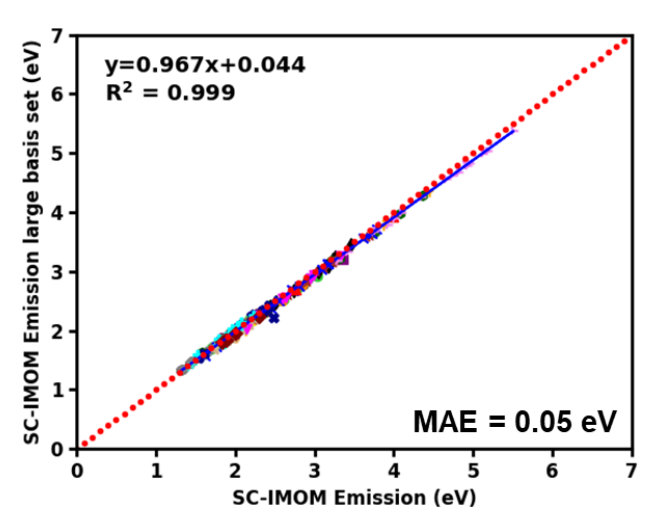


**Figure 9**: Comparison of SC-IMOM emission energies using Def2SVP and a large basis set (Def2TZVP). Both calculations used the same functional (B3LYP-D3BJ) and structure (obtained using Def2SVP basis set). The PCAD-dataset is used for this. The color coding is according to **Figure 1**. The red dotted line indicates the Y=X line.

Generally, in modern computational chemistry, much larger basis sets (polarized triple zeta or larger) are used to obtain results to enable comparisons with experiment. However, for valence excited states, polarized double- $\zeta$  quality basis sets are often enough.<sup>59</sup> Nevertheless, it is good practice to test if the results obtained are converged with respect to change in basis set size. Thus, we performed SC-IMOM emission calculations (single point at Def2SVP optimized structure) using a triple- $\zeta$  basis set (Def2TZVP) and compared it to double- $\zeta$  quality basis set results (**Figure 9**). All the points in **Figure 9** are located on the diagonal Y=X line with a very small MAE (0.05 eV). Thus, the results at the double- $\zeta$  Def2SVP basis set can be considered adequate for our calibration. The reasonable performance at such a small basis set can be attributed to the relatively similar electronic distribution in the ground and lowest excited state from which emission often occurs (compared to states such as Rydberg excited states or core excitations). Since excitation energy in  $\Delta$ -SCF methods are obtain as difference in SCF energy of two different states, there may be some cancellation of errors leading to faster convergence with respect to the size of basis set.

# 3.2 Application to the Large-dataset

The results thus far indicate SC-IMOM accurately predicts emission maxima of chromophores belonging to several different families of dye molecules. However, the number of chromophores in the PCAD-dataset is very small compared to the chromophores in the literature. Emission

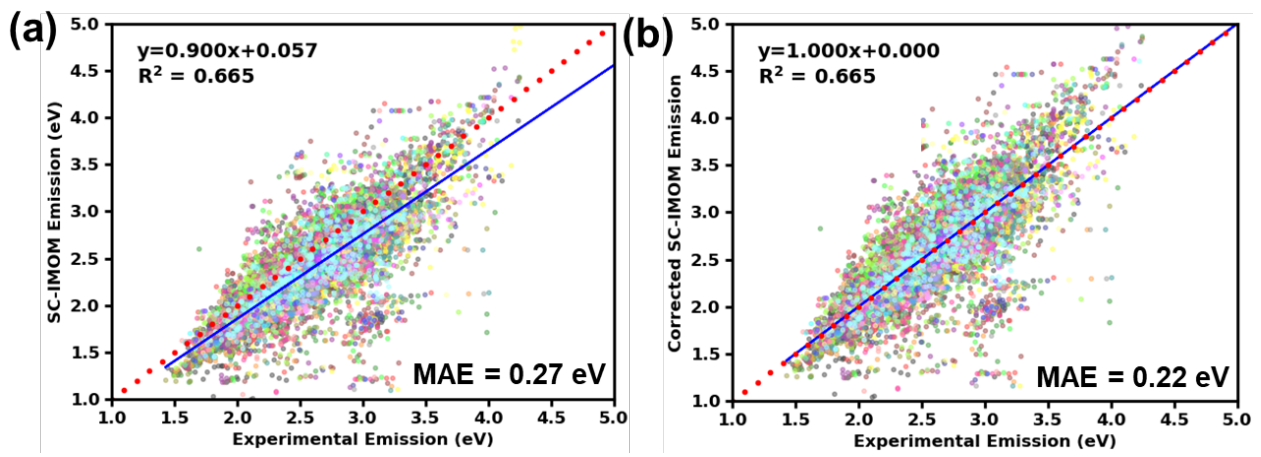


**Figure 10**: (a) Comparison of emission energies predicted by SC-IMOM to experimental emission maxima for the Large-dataset. The data points are color coded according to the solvent they are in (**Figure S6**). (b) The corrected SC-IMOM error is plotted against the experimental emission maxima. The corrections are performed using the linear fit equation in (a) as per **eq 8**. The red dotted line indicates the Y=X line.

energies for a broader range of molecules need to be obtained to verify the accuracy of SC-IMOM in predicting emission maxima for a variety of chromophores. To this end, we performed calculations on the Large-dataset containing a large number (4487) of different chromophores and solvents (69), forming a good representative dataset for all the chromophores in the literature.

The results for the comparison between SC-IMOM and experimental emission maxima on this Large-dataset is summarized in **Figure 10**. The data points in the scatter plot are colored as per the solvent and demonstrate no systematic dependence of the predicted error on solvation. The correlation between the predicted and experimental values were slightly lower (R<sup>2</sup> = 0.665), however, the corresponding errors were also slightly lower (MAE = 0.27 eV) compared to the PCAD-dataset. A large component (~40%) of the errors in the dataset lie between -0.1 and -0.3 eV, as illustrated by the histogram in **Figure S7a**. Thus, SC-IMOM using the B3LYP-D3BJ/Def2SVP level of theory marginally underpredicts emission. Overall, the performance of SC-IMOM is impressive when considering the target data is experimental instead of a high-level theoretical method, which is typically the case.

The theoretical predictions may be further improved by calibration, e.g., by adding a constant correction factor or using the best fit line (linear regression). The best fit line is more appropriate as it accounts for the systematic error in the data. The corrected theoretical prediction can be obtained as per the following equation:

Using the corrected prediction by linear regression, the error was reduced to 0.22 eV as shown by the lower CMAE (corrected mean absolute error) in **Figure 10(b)**. As expected, the linear regression line for the corrected prediction vs experimental value is the Y=X line with the correlation remaining unchanged. The errors resulting from the corrected predictions lie between -0.1 and 0.1 eV, as illustrated by the histogram in **Figure S7b** being centered around 0 eV.

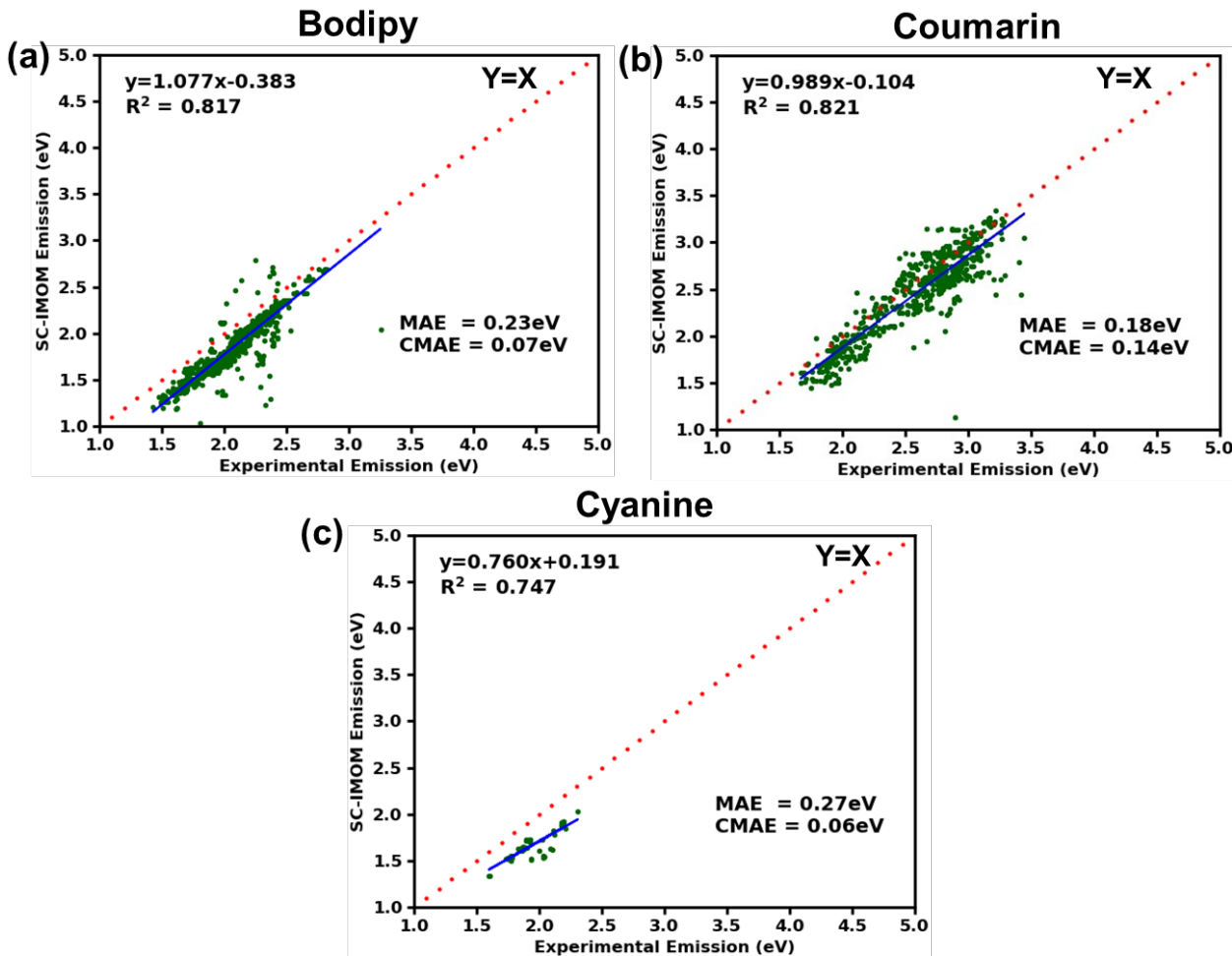


**Figure 11**: The datapoints corresponding to chromophores containing 3 common moieties such as (a) BODIPY, (b) Coumarin and (c) Cyanine are presented. The SMARTS expressions used to identify the dye classes are presented in **Table S1**. Note that molecules belonging to multiple dye classes are excluded here. The corrected MAE (CMAE) is calculated using the corresponding linear fit equations as per **eq 9**.

A further improvement in performance can potentially be achieved by correcting for the systematic errors in individual families of chromophores using a linear regression as per eq 9. This approach needs categorization of chromophores into their corresponding dye families. We used SMARTS patterns to identify chromophores belonging to the 13 most common dye classes (**Table** 

**S1**). BODIPY and carbazole were the most and least represented dye class, appearing 1040 and 54 times, respectively, in the Large-dataset. **Figure 11** presents the calculated vs experimental emission of different chromophore-solvent pairs belonging to three out of the 13 dye classes. For other dye classes please refer to **Figure S8**. Note that the chromophores are chosen such that they belong to only one of these dye classes. Chromophores belonging to multiple dye classes were not considered in this classification. Since anthracene is a part of perylene, the chromophores belonging to the perylene dye class were not considered to belong to the anthracene dye family.

A large variation in performance of SC-IMOM is observed for the various dye classes with MAE's ranging from 0.09 eV for carbazole dyes to 0.47 eV for anthracene dyes. The corrected predictions using individual linear regressions of the dye classes improved performance significantly as per the lower CMAE compared to MAE for all the dye classes. The improvement in performance due to the correction was most significant for the cyanine dyes, from 0.27 eV to 0.06 eV, due to the systematic underprediction. The results for chromophore-solvent pairs belonging to one of the 13 dye classes are shown in **Figure 12**. Using this additional categorization of the dye classes, we improved the CMAE from 0.22 eV (**Figure 10b**) to 0.17 eV (**Figure 12b**).

## 3.3 Using IMOM spin density to classify chromophores into dye classes

The linear regression line for the corrected prediction falls along the Y=X line in **Figure 12b**. However, unlike **Figure 10**, there is an improvement in the correlation. This improvement is due

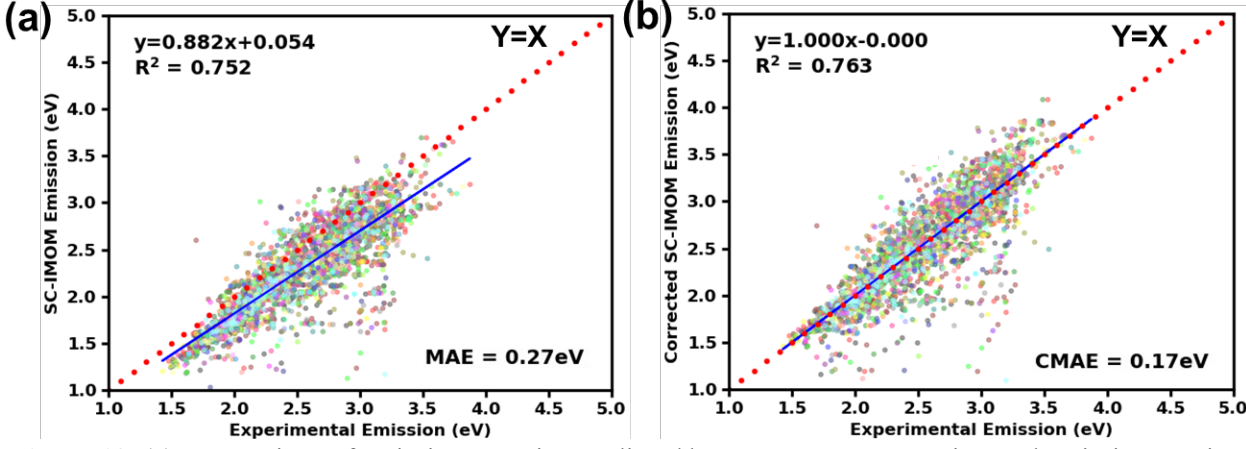
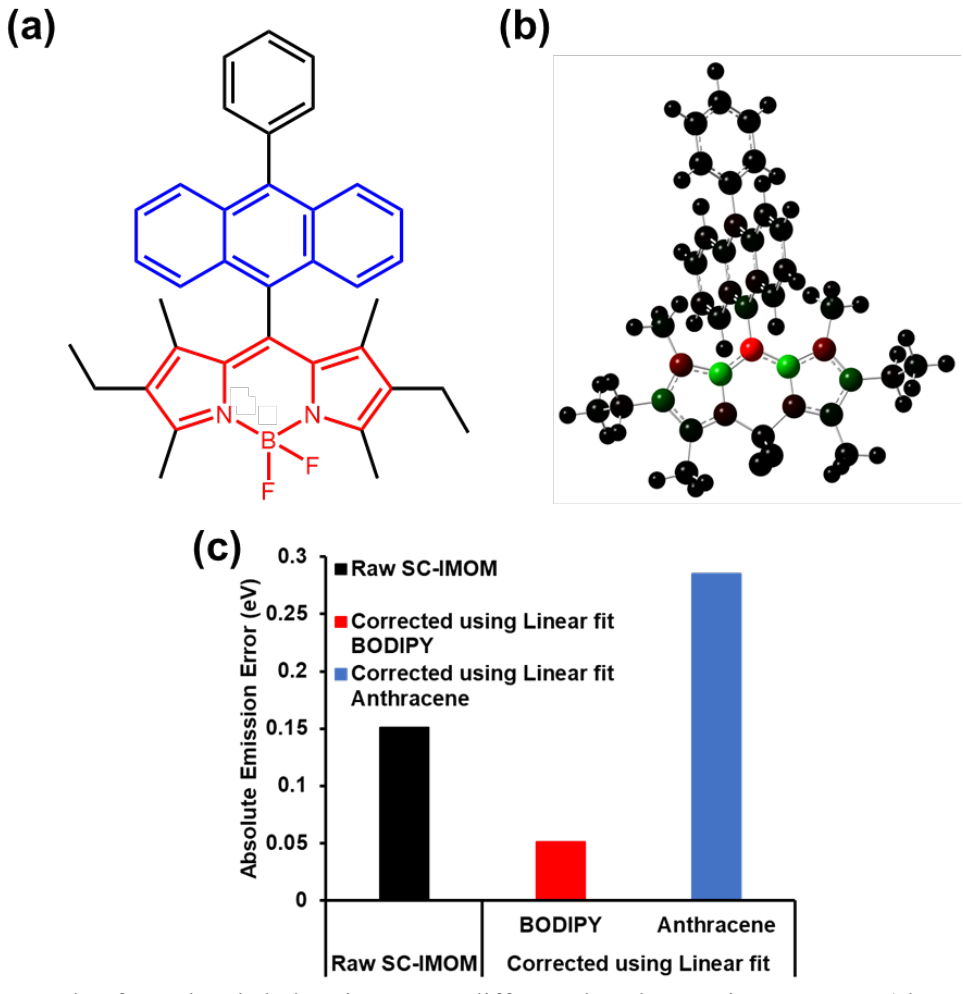


Figure 12: (a) Comparison of emission energies predicted by SC-IMOM to experimental emission maxima for the part of Large-dataset belonging to one of the 13 dye classes in **Table S1**. The data points are color coded according to the solvent they are in as per **Figure S6**. (b) The corrected SC-IMOM error is plotted against the experimental emission maxima. The corrections are performed using the linear fit equations of individual dye classes in **Figures 11** and **S8** as per **eq 9**. The red dotted line indicates the y=x line.

to the separate correction used for each class of dye. This impressive performance could be achieved for chromophores that could be categorized into one of the dye classes. However, such a classification is complex in general. Specifically, for chromophores containing moieties from multiple dye classes, the use of structural features is not sufficient. In such cases, electronic features, such as, natural transition orbitals<sup>60</sup> (NTO), are widely used to identify the character of the electronic transitions in TDDFT.<sup>61-64</sup> Thus, TDDFT, being a linear response method, requires the calculation of NTOs for a concise identification of the excited states.

Unlike TDDFT, IMOM obtains the excited state orbitals. Thus, IMOM can identify the excited state properties directly. To demonstrate this idea, we chose a substituted BODIPY-anthracene



**Figure 13**: (a) Example of a molecule belonging to two different dye classes viz., BODIPY (shown in red) and anthracene (shown in blue). (b) IMOM Mulliken spin density at the excited state geometry. The spin density in red and green denotes negative and positive spin density respectively. (c) Comparison of raw SC-IMOM and corrected SC-IMOM emission energies using either BODIPY or anthracene linear fit in **Figures 11a** or **S8c** respectively with experimental emission maxima.

dyad (BAD) (**Figure 13a**). Using only structural features, this chromophore belongs to both the BODIPY and anthracene dye families. Filatov *et al.* attributed the emission of this BAD to a "local emission" of the BODIPY chromophore with the first excited state (S<sub>1</sub>) being a  $\pi \rightarrow \pi^*$  excitation.<sup>65</sup> The IMOM Mulliken spin density (**Figure 13b**) agrees well with the previous report. Identification of the dye class using spin density can be utilized along with the correction based on categorization into dye classes to improve the raw SC-IMOM predicted emission as illustrated in **Figure 13c**. The raw error of SC-IMOM was calculated to be 0.15 eV. Using the correction from the spin density that assigns the BAD emission to BODIPY dye class helped improve the performance by reducing the error to 0.05 eV. In contrast, if BAD was assigned to the anthracene dye class, the performance worsened with an increased error of 0.29 eV.

Thus, accurate classification of the S<sub>1</sub> excited state / emissive state to a single chromophore class is critical in obtaining higher accuracy using linear fit-based corrections. The accuracy of these corrections can also be improved by adding more chromophore-solvent pairs or improving the dye identification strategies. Further improvement in performance may require machine learning models as they do not need explicit detection of dye classes. These ideas will be the focus of future work.

# 3.4 Analysis of the convergence behavior of IMOM excited state SCF calculations

Δ-SCF methods can be employed as alternative to canonical excited state methods such as TDDFT.<sup>31, 66</sup> However, methods such as IMOM which facilitate SCF calculations on electronic excited states not the lowest energy of a given symmetry tend to have more difficulties to achieve SCF convergence. In principle, convergence can be achieved by changing the SCF algorithm of choice such as direct optimization,<sup>22</sup> level shifting<sup>21</sup> and minimizing square of the gradient,<sup>25</sup> etc. While we have not explored the convergence performance of such alternate algorithms, we have performed a limited analysis of our current results to identify and understand the chemical space of systems where difficulties in convergence have been observed thus far.

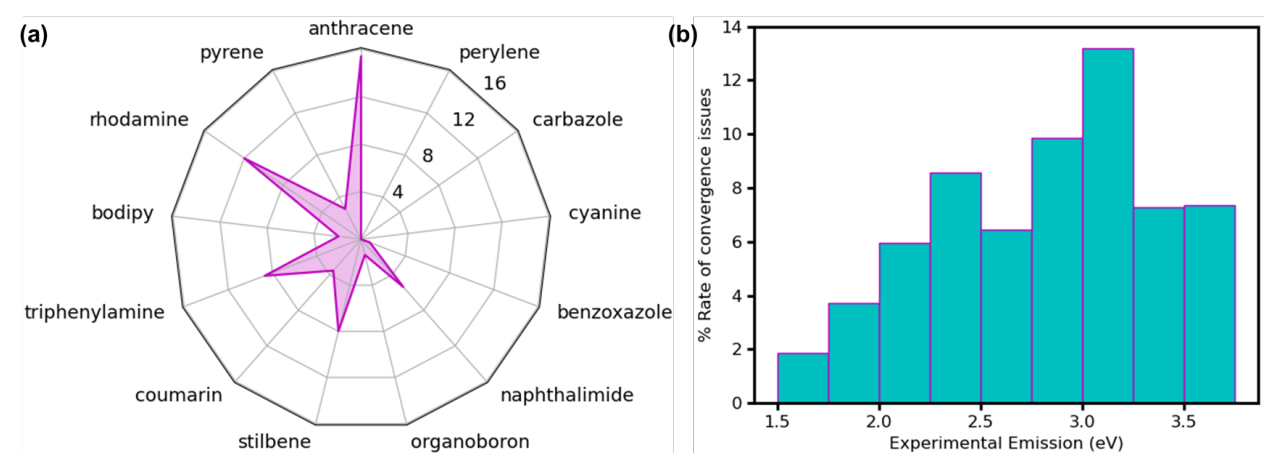


**Figure 14**: (a) and (b) present the percentage of chromophore-solvent combinations in the large-dataset whose IMOM excited state optimization did not converge for different dye classes and range of emission maxima respectively. The results for dye classes are presented for all the chromophores that could be classified uniquely into one of the 13 dyes classes in **Table S1**. The range of experimental emission is limited to [1.5 eV, 3.75 eV) range where enough data is available.

We take advantage of the large dye chemical space coverage of the Large-dataset to make meaningful assertions. In total 7% (975 out of 13,293) chromophore-solvent combinations had excited state SCF convergence issue during IMOM excited state optimization. The rate of convergence (93%) is much higher than our initial expectations since we are performing calculations on excited state structures away from equilibrium and many different solvents (69). The variation in the rate of chromophores with convergence issues in different dye classes is presented in **Figure 14a**. Anthracene dyes had the most convergence issues (15%). On the other hand, perylene, cyanine and carbazole dyes did not have any convergence issues. The 100% convergence of these three dye classes could be partly attributed to the fewer number of data points (less than 100) in those three dye classes. Overall, in the majority of dye classes the rate of convergence issues was lower than 4%, including Bodipy with more than 1000 chromophore-solvent pairs.

Further, we investigated the dependence of the rate of convergence issues on the emission maxima. The results are presented in **Figure 14b**. At lower energy emission region there are fewer issues (less than 2%). The rate of convergence issues increases going to higher energy range of the spectrum peaking around 3 eV. The rate of convergence issues correlates well with the SC-IMOM error which also increases, in magnitude, with increasing emission energy peaking around 3 eV

(**Figure S9**). Thus, uncorrected IMOM has better and more reliable performance in the lower energy range of the visible spectrum.

#### 4. Conclusions

The  $\Delta$ -SCF method, IMOM, accelerated the prediction of emission maxima for the purpose of screening large numbers of dye molecules. Small (205) and large (12,318) datasets were employed to show the generality of our observations. Using IMOM, we were able to obtain S<sub>1</sub> excited state structures and emission energies using an automated procedure, making the process black box. While IMOM underestimated excitation energies, a spin corrected version (SC-IMOM) significantly improved the accuracy. Since emission generally takes place from the first singlet excited state (Kasha's rule), we demonstrated that optimization of the S<sub>1</sub> excited state accurately reproduced experimental emission energies with MAE of 0.30 and 0.27 eV for the small and large datasets containing diverse sets of chromophores. We classified the contents of the large dataset into chromophores belonging to 13 different common dye classes, further lowering MAE to 0.17 eV for chromophores belonging to several popular dye classes. We demonstrated the ability of IMOM spin density to identify the dye class of a complex chromophore dyad with structural moieties from two different dye classes. Finally, we show that the rate of convergence of IMOM excited state SCF calculations has small but significant variations among the different dye classes and emission energy. The analysis revealed that anthracene dye class has the most convergence issues and generally convergence issues increased with higher emission energy peaking around 3 eV. The accuracy of the predicted emission energies, the unsupervised nature of the method, and the economy of calculations showcase the potential for SC-IMOM in the design of optical materials with desirable emission properties.

# **Supporting Information**

The supporting information contains tables, figures, coordinates, numerical data and python script used to generate the initial conformations of the Large-dataset. The supporting information is available free of charge on the journal website.

### Acknowledgements

We thank Dr. Daniel A. Beckett for his contribution toward the implementation of IMOM in our version of Gaussian. We thank Dr. Tumpa Sadhukhan for many scientific discussions in the early

stages of planning this work. This project was supported by the National Science Foundation, Designing Materials to Revolutionize and Engineer the Future Program (Grant: DMR-2118423) at Indiana University. The Big Red 3 supercomputing facility at Indiana University was used for most of the calculations in this study.

#### References

- 1. Benson, C. R.; Kacenauskaite, L.; VanDenburgh, K. L.; Zhao, W.; Qiao, B.; Sadhukhan, T.; Pink, M.; Chen, J. S.; Borgi, S.; Chen, C. H.; Davis, B. J.; Simon, Y. C.; Raghavachari, K.; Laursen, B. W.; Flood, A. H., Plug-and-Play Optical Materials from Fluorescent Dyes and Macrocycles. *Chem* **2020**, *6*, 1978-1997.
- 2. Qu, L.; Zhou, X.; Song, J.; Zhang, B.; Yang, Q.; Zhou, X.; Liu, J.; Xiang, H., Circularly Polarized Luminescence Switching, Chirality Self-Sorting, and Cell Imaging of Chiral Rhodamine Dyes. *Adv Optical Mater* **2023**, *11*, 2300779.
- 3. Gray, V.; Dzebo, D.; Abrahamsson, M.; Albinsson, B.; Moth-Poulsen, K., Triplet-triplet annihilation photon-upconversion: towards solar energy applications. *Physical Chemistry Chemical Physics* **2014**, *16*, 10345-10352.
- 4. Walter, B., Die Aenderung des Fluorescenzvermögens mit der Concentration. *Annalen der Physik* **1888**, *270*, 316-326.
- 5. Dexter, D. L.; Schulman, J. H., Theory of Concentration Quenching in Inorganic Phosphors. *The Journal of Chemical Physics* **2004**, *22*, 1063-1070.
- 6. Chen, J. S.; Fateminia, S. M. A.; Kacenauskaite, L.; Bærentsen, N.; Stenspil, S. G.; Bredehoeft, J.; Martinez, K. L.; Flood, A. H.; Laursen, B. W., Ultrabright Fluorescent Organic Nanoparticles Based on Small-Molecule Ionic Isolation Lattices. *Angew Chem Int Ed* **2021**, *60*, 9450-9458.
- 7. Nishiyama, R.; Furuya, K.; McCann, P.; Kacenauskaite, L.; Laursen, B. W.; Flood, A. H.; Hiramatsu, K.; Goda, K., Boosting the Brightness of Raman Tags Using Cyanostar Macrocycles. *Anal Chem* **2023**, *95*, 12835-12841.
- 8. Szczypinski, F. T.; Bennett, S.; Jelfs, K. E., Can we predict materials that can be synthesised? *Chem Sci* **2021**, *12*, 830-840.
- 9. Bruns, R. F.; Watson, I. A., Rules for Identifying Potentially Reactive or Promiscuous Compounds. *J Med Chem* **2012**, *55*, 9763-9772.
- 10. Mukherjee, D.; Mukherjee, P. K., Response-Function Approach to the Direct Calculation of the Transition-Energy in a Multiple-Cluster Expansion Formalism. *Chem Phys* **1979**, *39*, 325-335.
- 11. Siegbahn, P.; Heiberg, A.; Roos, B.; Levy, B., Comparison of the Super-Cl and the Newton-Raphson Scheme in the Complete Active Space Scf Method. *Phys Scripta* **1980**, *21*, 323-327.
- 12. Vogiatzis, K. D.; Ma, D. X.; Olsen, J.; Gagliardi, L.; de Jong, W. A., Pushing configuration-interaction to the limit: Towards massively parallel MCSCF calculations. *J Chem Phys* **2017**, *147*, 184111.
- 13. Fan, P. D.; Valiev, M.; Kowalski, K., Large-scale parallel calculations with combined coupled cluster and molecular mechanics formalism: Excitation energies of zinc-porphyrin in aqueous solution. *Chem Phys Lett* **2008**, *458*, 205-209.
- 14. Runge, E.; Gross, E. K. U., Density-Functional Theory for Time-Dependent Systems. *Physical Review Letters* **1984**, *52*, 997-1000.
- 15. Bagus, P. S., Self-Consistent-Field Wave Functions for Hole States of Some Ne-Like and Ar-Like Ions. *Phys Rev* **1965**, *139*, A619-A634.

- 16. Hedin, L.; Johansso.A, Polarization Corrections to Core Levels. *J Phys Pt B Atom M P* **1969**, 2, 1336-1346.
- 17. Hunt, W. J.; Goddard, W. A., Excited states of H2O using improved virtual orbitals. *Chem Phys Lett* **1969**, *3*, 414-418.
- 18. Huzinaga, S.; Arnau, C., Virtual Orbitals in Hartree-Fock Theory. *Phys Rev A* **1970**, *1*, 1285-1288.
- 19. Huzinaga, S.; Arnau, C., Virtual Orbitals in Hartree-Fock Theory. II. *J Chem Phys* **1971**, *54*, 1948-1951.
- 20. Morokuma, K.; Iwata, S., Extended Hartree-Fock Theory for Excited-States. *Chem Phys Lett* **1972**, *16*, 192-197.
- 21. Carter-Fenk, K.; Herbert, J. M., State-Targeted Energy Projection: A Simple and Robust Approach to Orbital Relaxation of Non-Aufbau Self-Consistent Field Solutions. *J Chem Theory Comput* **2020**, *16*, 5067-5082.
- 22. Levi, G.; Ivanov, A. V.; Jónsson, H., Variational Density Functional Calculations of Excited States via Direct Optimization. *J Chem Theory Comput* **2020**, *16*, 6968-6982.
- 23. Gilbert, A. T. B.; Besley, N. A.; Gill, P. M. W., Self-Consistent Field Calculations of Excited States Using the Maximum Overlap Method (MOM). *J Phys Chem A* **2008**, *112*, 13164-13171.
- 24. Barca, G. M. J.; Gilbert, A. T. B.; Gill, P. M. W., Simple Models for Difficult Electronic Excitations. *J Chem Theory Comput* **2018**, *14*, 1501-1509.
- 25. Hait, D.; Head-Gordon, M., Excited State Orbital Optimization via Minimizing the Square of the Gradient: General Approach and Application to Singly and Doubly Excited States via Density Functional Theory. *J Chem Theory Comput* **2020**, *16*, 1699-1710.
- 26. Barca, G. M. J.; Gilbert, A. T. B.; Gill, P. M. W., Excitation Number: Characterizing Multiply Excited States. *J Chem Theory Comput* **2018**, *14*, 9-13.
- 27. Cheng, C. L.; Wu, Q.; Van Voorhis, T., Rydberg energies using excited state density functional theory. *J Chem Phys* **2008**, *129*, 124112.
- 28. Hait, D.; Head-Gordon, M., Highly Accurate Prediction of Core Spectra of Molecules at Density Functional Theory Cost: Attaining Sub-electronvolt Error from a Restricted Open-Shell Kohn-Sham Approach. *J Phys Chem Lett* **2020**, *11*, 775-786.
- 29. Zamani, A. Y.; Hratchian, H. P., Δ-based composite models for calculating x-ray absorption and emission energies. *The Journal of Chemical Physics* **2023**, *159*, 224109.
- 30. Briggs, E. A.; Besley, N. A.; Robinson, D., QM/MM Excited State Molecular Dynamics and Fluorescence Spectroscopy of BODIPY. *J Phys Chem A* **2013**, *117*, 2644-2650.
- 31. Kowalczyk, T.; Yost, S. R.; Van Voorhis, T., Assessment of the ΔSCF density functional theory approach for electronic excitations in organic dyes. *J Chem Phys* **2011**, *134*, 054128.
- 32. Taniguchi, M.; Du, H.; Lindsey, J. S., PhotochemCAD 3: Diverse Modules for Photophysical Calculations with Multiple Spectral Databases. *Photochem Photobiol* **2018**, *94*, 277-289.
- 33. Nakata, M.; Shimazaki, T., PubChemQC Project: A Large-Scale First-Principles Electronic Structure Database for Data-Driven Chemistry. *J Chem Inf Model* **2017**, *57*, 1300-1308.

- 34. Liang, J. C.; Ye, S. Q.; Dai, T. S.; Zha, Z. Y.; Gao, Y. C.; Zhu, X., QM-symex, update of the QM-sym database with excited state information for 173 kilo molecules. *Sci Data* **2020**, *7*, 400.
- 35. Wilbraham, L.; Smajli, D.; Heath-Apostolopoulos, I.; Zwijnenburg, M. A., Mapping the optoelectronic property space of small aromatic molecules. *Commun Chem* **2020**, *3*, 14.
- 36. Ramakrishnan, R.; Hartmann, M.; Tapavicza, E.; von Lilienfeld, O. A., Electronic spectra from TDDFT and machine learning in chemical space. *J Chem Phys* **2015**, *143*, 084111.
- 37. Verma, S.; Rivera, M.; Scanlon, D. O.; Walsh, A., Machine learned calibrations to high-throughput molecular excited state calculations. *J Chem Phys* **2022**, *156*, 134116.
- 38. Westermayr, J.; Gilkes, J.; Barrett, R.; Maurer, R. J., High-throughput property-driven generative design of functional organic molecules. *Nat Comput Sci* **2023**, *3*, 139-148.
- 39. Kang, B.; Seok, C.; Lee, J., Prediction of Molecular Electronic Transitions Using Random Forests. *J Chem Inf Model* **2020**, *60*, 5984-5994.
- 40. Grimme, S.; Bannwarth, C., Ultra-fast computation of electronic spectra for large systems by tight-binding based simplified Tamm-Dancoff approximation (sTDA-xTB). *J Chem Phys* **2016**, *145*, 054103.
- 41. Christiansen, O.; Koch, H.; Jorgensen, P., The 2nd-Order Approximate Coupled-Cluster Singles and Doubles Model Cc2. *Chem Phys Lett* **1995**, *243*, 409-418.
- 42. Joung, J. F.; Han, M.; Jeong, M.; Park, S., Experimental database of optical properties of organic compounds. *Sci Data* **2020**, *7*, 295.
- 43. Weininger, D., SMILES, a chemical language and information system. 1. Introduction to methodology and encoding rules. *J Chem Inf Comput Sci* **1988**, *28*, 31-36.
- 44. Frisch, M. J.; Trucks, G. W.; Schlegel, H. B.; Scuseria, G. E.; Robb, M. A.; Cheeseman, J. R.; Scalmani, G.; Barone, V.; Petersson, G. A.; Nakatsuji, H.; Li, X.; Caricato, M.; Marenich, A. V.; Bloino, J.; Janesko, B. G.; Gomperts, R.; Mennucci, B.; Hratchian, H. P.; Ortiz, J. V.; Izmaylov, A. F.; Sonnenberg, J. L.; Williams; Ding, F.; Lipparini, F.; Egidi, F.; Goings, J.; Peng, B.; Petrone, A.; Henderson, T.; Ranasinghe, D.; Zakrzewski, V. G.; Gao, J.; Rega, N.; Zheng, G.; Liang, W.; Hada, M.; Ehara, M.; Toyota, K.; Fukuda, R.; Hasegawa, J.; Ishida, M.; Nakajima, T.; Honda, Y.; Kitao, O.; Nakai, H.; Vreven, T.; Throssell, K.; Montgomery Jr., J. A.; Peralta, J. E.; Ogliaro, F.; Bearpark, M. J.; Heyd, J. J.; Brothers, E. N.; Kudin, K. N.; Staroverov, V. N.; Keith, T. A.; Kobayashi, R.; Normand, J.; Raghavachari, K.; Rendell, A. P.; Burant, J. C.; Iyengar, S. S.; Tomasi, J.; Cossi, M.; Millam, J. M.; Klene, M.; Adamo, C.; Cammi, R.; Ochterski, J. W.; Martin, R. L.; Morokuma, K.; Farkas, O.; Foresman, J. B.; Fox, D. J. Gaussian Development Version, Wallingford, CT, 2016.
- 45. Stephens, P. J.; Devlin, F. J.; Chabalowski, C. F.; Frisch, M. J., Ab-Initio Calculation of Vibrational Absorption and Circular-Dichroism Spectra Using Density-Functional Force-Fields. *The Journal of Physical Chemistry* **1994**, *98*, 11623-11627.
- 46. Weigend, F.; Ahlrichs, R., Balanced basis sets of split valence, triple zeta valence and quadruple zeta valence quality for H to Rn: Design and assessment of accuracy. *Physical Chemistry Chemical Physics* **2005**, *7*, 3297-3305.
- 47. Kasha, M., Characterization of electronic transitions in complex molecules. *Discussions of the Faraday Society* **1950**, *9*, 14-19.

- 48. Ziegler, T.; Rauk, A.; Baerends, E. J., On the calculation of multiplet energies by the hartree-fock-slater method. *Theoretica chimica acta* **1977**, *43*, 261-271.
- 49. Noodleman, L., Valence bond description of antiferromagnetic coupling in transition metal dimers. *The Journal of Chemical Physics* **1981**, *74*, 5737-5743.
- 50. Yamaguchi, K.; Fukui, H.; Fueno, T., MOLECULAR ORBITAL (MO) THEORY FOR MAGNETICALLY INTERACTING ORGANIC COMPOUNDS. AB-INITIO MO CALCULATIONS OF THE EFFECTIVE EXCHANGE INTEGRALS FOR CYCLOPHANE-TYPE CARBENE DIMERS. *Chemistry Letters* **1986**, *15*, 625-628.
- 51. Schreiner, E.; Nair, N. N.; Pollet, R.; Staemmler, V.; Marx, D., Dynamical magnetostructural properties of Anabaena ferredoxin. *Proceedings of the National Academy of Sciences* **2007**, *104*, 20725-20730.
- 52. Hratchian, H. P., Communication: An efficient analytic gradient theory for approximate spin projection methods. *The Journal of Chemical Physics* **2013**, *138*, 101101.
- 53. Hanson-Heine, M. W. D.; Wriglesworth, A.; Uroos, M.; Calladine, J. A.; Murphy, T. S.; Hamilton, M.; Clark, I. P.; Towrie, M.; Dowden, J.; Besley, N. A.; George, M. W., Calculating singlet excited states: Comparison with fast time-resolved infrared spectroscopy of coumarins. *J Chem Phys* **2015**, *142*, 154119.
- 54. Hanson-Heine, M. W. D.; George, M. W.; Besley, N. A., Calculating excited state properties using Kohn-Sham density functional theory. *J Chem Phys* **2013**, *138*, 064101.
- 55. Karaman, O.; Alkan, G. A.; Kizilenis, C.; Akgul, C. C.; Gunbas, G., Xanthene dyes for cancer imaging and treatment: A material odyssey. *Coordination Chemistry Reviews* **2023**, *475*, 214841.
- 56. Zeng, S.; Liu, X. S.; Kafuti, Y. S.; Kim, H.; Wang, J. Y.; Peng, X. J.; Li, H. D.; Yoon, J., Fluorescent dyes based on rhodamine derivatives for bioimaging and therapeutics: recent progress, challenges, and prospects. *Chem Soc Rev* **2023**, *52*, 5607-5651.
- 57. Cerdán, L.; Martínez-Martínez, V.; García-Moreno, I.; Costela, A.; Pérez-Ojeda, M. E.; Arbeloa, I. L.; Wu, L. X.; Burgess, K., Naturally Assembled Excimers in Xanthenes as Singular and Highly Efficient Laser Dyes in Liquid and Solid Media. *Adv Optical Mater* **2013**, *1*, 984-990.
- 58. Leang, S. S.; Zahariev, F.; Gordon, M. S., Benchmarking the performance of time-dependent density functional methods. *J Chem Phys* **2012**, *136*.
- 59. Elliott, P.; Furche, F.; Burke, K., Excited States from Time-Dependent Density Functional Theory. *Rev Comp Ch* **2009**, *26*, 91-165.
- 60. Martin, R. L., Natural transition orbitals. *J Chem Phys* **2003**, *118*, 4775-4777.
- 61. Zhang, K.; Wang, X.; Cai, L.; Fan, J.; Wang, C.-K.; Lin, L., Theoretical study on the influence of substitution position on the luminescence properties and charge transfer characteristics of thermally activated delayed fluorescent molecules. *Spectrochimica Acta Part A: Molecular and Biomolecular Spectroscopy* **2024**, *308*, 123718.
- 62. Budyka, M. F., Density functional theory study of the styrylbenzoquinoline dyad and the related dibenzoquinolylcyclobutane formed in the [2+2] photocycloaddition reaction. *Int J Quantum Chem* **2024**, *124*, e27264.

- 63. Titov, E.; Beqiraj, A., Exciton States of Azobenzene Aggregates: A First-Principles Study. *Adv Theor Simul* **2023**, *6*, 2200907.
- 64. Tecuapa-Flores, E. D.; Palacios-Cabrera, C. B.; Santiago-Cuevas, A. J.; Hernández, J. G.; Narayanan, J.; Thangarasu, P., Simultaneous recognition of dopamine and uric acid in real samples through highly sensitive new electrode fabricated using ZnO/carbon quantum dots: bio-imaging and theoretical studies. *Analyst* **2023**, *149*, 108-124.
- 65. Filatov, M. A.; Karuthedath, S.; Polestshuk, P. M.; Callaghan, S.; Flanagan, K. J.; Telitchko, M.; Wiesner, T.; Laquai, F.; Senge, M. O., Control of triplet state generation in heavy atom-free BODIPY-anthracene dyads by media polarity and structural factors. *Physical Chemistry Chemical Physics* **2018**, *20*, 8016-8031.
- 66. Worster, S. B.; Feighan, O.; Manby, F. R., Reliable transition properties from excited-state mean-field calculations. *J Chem Phys* **2021**, *154*, 124106.